Advanced oxidation protein products aggravate age-related bone loss by increasing sclerostin expression in osteocytes via ROS-dependent downregulation of Sirt1

JIHUAN ZENG[1,2], QIANG XIAO[2], XIAODAN LI[3] and JIANTING CHEN[1]

[1]Department of Orthopaedics and Spine Surgery, Nanfang Hospital, Southern Medical University, Guangzhou, Guangdong 510515; [2]Department of Orthopeadics, Jiangxi Provincial People's Hospital Affiliated to Nanchang University, Nanchang, Jiangxi 330006; [3]Department of Nursing, Jiangxi Health Vocational College, Nanchang, Jiangxi 330052, P.R. China

Received January 11, 2021; Accepted March 11, 2021

DOI: 10.3892/ijmm.2021.4941

Abstract. Advanced oxidation protein products (AOPPs) induce intracellular oxidative stress (OS) and are involved in numerous diseases. AOPPs accumulate with age, and our previous study revealed that AOPPs accelerated bone deterioration in aged rats. However, the underlying mechanism remains unknown. The present study demonstrated that AOPPs aggravated bone loss in aging male mice by increasing the resorptive activity and decreasing the formative activity of bone tissues. In addition, *SOST* mRNA (encoding sclerostin) and sclerostin protein levels were increased in the bone tissues of AOPP-treated mice, which was associated with enhanced OS status as well as decreased Sirtuin 1 (*SIRT1*) mRNA and protein expression levels. Incubation of MLO-Y4 cells with AOPPs induced the accumulation of reactive oxygen species (ROS) via the activation of nicotinamide adenine dinucleotide phosphate (NADPH) oxidases. The accumulated ROS then upregulated sclerostin expression in MLO-Y4 cells by decreasing Sirt1 expression. *In vivo*, AOPP-challenged mice co-treated with apocynin (an inhibitor of NADPH oxidases), N-acetyl-L-cysteine (a ROS scavenger) or SRT3025 (a Sirt1 activator) displayed improved bone mass and microstructure. Moreover, sclerostin expression in the bone tissues of the co-treated groups was significantly lower compared with that in groups treated with AOPPs alone. Collectively, these data suggested that AOPPs aggravated age-related bone loss by increasing the expression of sclerostin in osteocytes via ROS-dependent downregulation of Sirt1. The present findings provide novel insights into the pathogenesis of senile osteoporosis.

Correspondence to: Dr Jianting Chen, Department of Orthopaedics and Spine Surgery, Nanfang Hospital, Southern Medical University, 1838 North Guangzhou Avenue, Guangzhou, Guangdong 510515, P.R. China
E-mail: chenjt99@tom.com

Key words: advanced oxidation protein products, age-related bone loss, sclerostin, oxidative stress, sirtuin 1

Introduction

Bone homeostasis depends on an intricate coupling between bone formation and resorption (1). Age-related bone loss is one main cause of fractures in the elderly population, which is characterized by reduced bone formation but persistent bone resorption (2). Despite considerable progress in research on the pathophysiology of osteoporosis over the past several decades, the underlying mechanisms of defective bone coupling in age-related bone loss remain poorly understood.

Terminally differentiated and, matrix-embedded osteocytes, which are regarded as the orchestrators of bone remodeling, regulate the activities of osteoblasts and osteoclasts (3). An important factor of the osteocytic regulation of bone metabolism is sclerostin, a Wnt/β-catenin antagonist (4). Previous studies have reported that sclerostin can largely affect bone homeostasis by decreasing bone formation but increasing bone resorption (5,6). Plasma sclerostin levels increase with age, and are associated with low bone mass and osteoporotic fracture (7,8). Moreover, treatment with an anti-sclerostin-neutralizing antibody has been revealed to restore bone mass and strength in aged rats (9). Thus, considering these findings, it can be inferred that elevated levels of sclerostin during aging, may contribute to age-related bone loss.

Reactive oxygen species (ROS), which include hydroxyl radicals, superoxides and hydrogen peroxides (H_2O_2), are important secondary messengers and serve essential roles in multiple physiological cellular responses at their normal low levels (10). However, excessive intracellular ROS result in oxidative stress (OS), which damages biomolecules, including proteins, lipids, and nucleotides (11). Advanced oxidation protein products (AOPPs) are cross-linked proteins enriched in dityrosine, which are formed by the reaction of plasma proteins with chlorinated compounds during OS (12,13). The accumulation of AOPPs occurs in numerous redox-related diseases, such as chronic kidney diseases, diabetes, inflammatory bowel diseases, rheumatoid arthritis, postmenopausal osteoporosis,

and spinal cord injury. AOPPs are regarded as new biomarkers of OS (14-19). However, previous studies have revealed that AOPPs are not only the byproducts of OS, but also induce intracellular OS by triggering NADPH oxidases in various cell types, and promote numerous diseases (14,16,19-22).

Our previous study reported that the level of AOPPs in plasma increased with age and was negatively correlated with bone mass in rats (23). Furthermore, it was revealed that AOPPs accelerated the loss of bone mass and microstructure degeneration in aged rats (24). However, the exact cellular basis of age-related bone loss induced by AOPPs remains unknown. The present study demonstrated that AOPPs aggravated age-related bone loss by increasing the expression of sclerostin in osteocytes via the downregulation of sirtuin 1 (Sirt1), and this process was induced by NADPH oxidases dependent of ROS generation.

Materials and methods

Mice and reagents. Male C57Bl/6 mice (age, 12 months) were obtained from Chengdu Dashuo Laboratory Animal Co., Ltd. The MLO-Y4 mouse-derived osteocytic cell line (derived from long bones of mice) was purchased from PythonBio (http://www.pythonbiotech.com). Fetal bovine serum (FBS), calf serum (CS), and α-minimum essential medium (α-MEM) were purchased from Thermo Fisher Scientific, Inc. A Cell Counting Kit-8 (CCK-8) assay was purchased from Dojindo Molecular Technologies, Inc. The ROS assay kit was purchased from Beyotime Institute of Biotechnology. Primary antibodies against glyceraldehyde-3-phosphate dehydrogenase (GAPDH) (product code ab9485), sclerostin (product code ab63097), and Sirt1 (product code ab12193) were purchased from Abcam. Goat anti-rabbit secondary antibody conjugated with Cy3 (cat. no. SA00009-2) was purchased from ProteinTech Group, Inc. Horseradish peroxidase (HRP)-conjugated secondary antibodies (product code FD0155) and protease inhibitor tablets were purchased from Fude Biological Technology Co. Ltd. Apocynin, which is an inhibitor of nicotinamide adenine dinucleotide phosphate (NADPH) oxidases, N-acetyl-L-cysteine (NAC), which is an ROS scavenger, fluorescein diacetate (FDA) and bovine serum albumin (BSA) were obtained from Sigma-Aldrich; Merck KGaA. The Sirt1 activator, SRT3025, was purchased from Selleck Chemicals.

Preparation of AOPPs-BSA and concentration determination of AOPPs. AOPPs-BSA was prepared as previously described (12,24). Briefly, 20 mg/ml BSA was incubated (at 37˚C for 30 min) with 40 mM hypochlorous acid (HOCl) and diluted using phosphate-buffered saline (PBS, pH 7.4). To remove free HOCl, the mixed solution was dialyzed in PBS at 4˚C for 24 h. The controls used were BSA and PBS alone. Furthermore, a Detoxi-Gel column (Pierce; Thermo Fisher Scientific, Inc.) was used to remove contaminated endotoxins from all the samples. The endotoxin levels in the obtained samples were measured using a Limulus Amebocyte Lysate kit (Sigma; Merck KGaA) and a level of <0.05 ng/mg was considered as acceptable. Content of AOPPs in the sample was determined as previously described (12).

Animal treatment protocols. In total, 56 male C57Bl/6 mice (age, 12 months; body weight, 33.5±3.1 g) were used. All mice were maintained at 23˚C and 50-70% humidity with a 12-h light/dark cycle and were provided with free access to food and water. All animal experiments were approved (approval no. NFYY-2018-68) by the Laboratory Animal Care and Use Committee of Nanfang Hospital, Southern Medical University (Guangzhou, China).

The animal study consisted of two independent experiments. For the AOPPs-BSA interventional experiment, 28 mice matched by body weight were randomized into four groups (7 mice in each group) and subjected to the following treatments: Group 1, intraperitoneal (i.p.) injection of vehicle (PBS, pH 7.4); Group 2, i.p. injection of native BSA at 50 mg/kg/day; Group 3, i.p. injection of AOPPs-BSA at 50 mg/kg/day; and Group 4, i.p. injection of AOPPs-BSA at 100 mg/kg/day. For the blocking experiment, the remaining 28 mice were randomized into four groups and subjected to treatments as follows: Group 1, i.p. injection of AOPPs-BSA alone at 100 mg/kg/day; Group 2, i.p. injection of AOPPs-BSA at 100 mg/kg/day and apocynin at 100 mg/kg/day in drinking water; Group 3, i.p. injection of AOPPs-BSA at 100 mg/kg/day and NAC at 100 mg/kg/day in drinking water; Group 4, i.p. injection of AOPPs-BSA at 100 mg/kg/day and SRT3025 at 50 mg/kg/day in drinking water. After a treatment duration of 16 weeks, mice in each group were anesthetized using isoflurane (4% for induction, and 2.5% for maintenance), and blood samples were collected from the retroorbital vein (~500 μl blood was obtained from each mouse). Mice were then immediately sacrificed by standard cervical dislocation to avoid suffering. Subsequently, plasma was separated and stored at -80˚C. The tibia, femur and lumbar vertebra specimens were also obtained for further assessments.

Micro-CT analysis. The trabecular microstructure of L4 vertebral bodies and left proximal tibias were analyzed using micro-CT (μCT80; SCANCO Medical AG) at a resolution of 10 μm. The volume of interest (VOI) was defined as the entire trabecular bone region in the L4 vertebral body, and the trabecular bone region 100 slices downstream from the proximal growth plate of the tibia. The trabecular microstructure morphometric parameters, including bone volume over total volume (BV/TV), trabecular number (Tb.N), trabecular thickness (Tb.Th), and trabecular separation (Tb.Sp) were obtained via VOI analysis. All μCT analyses were performed in accordance with the guidelines of the American Society for Bone and Mineral Research (25).

Bone histological analysis and immunohistochemical staining. Tibial bone samples were fixed in 2% paraformaldehyde at 25˚C for 24 h, decalcified in 0.5 M EDTA (pH 7.5) for 3 weeks, and then embedded in paraffin. Osteoblast number and osteoclast area were measured on hematoxylin and eosin (H&E)-stained sections (5 μm) and tartrate-resistant acid phosphatase (TRAP)-stained sections (5 μm), respectively. For H&E-staining, paraffin sections were stained with hematoxylin for 2 min at 37˚C, followed by eosin for 5 min at 37˚C. For TRAP staining, paraffin sections were first reacted for TRAP activity (37˚C, 50 min) and then counterstained at 37˚C for 5 min with light green SF yellowfish solution (Merck KGaA,).

For immunohistochemical staining, paraffin sections (5 μm) were de-waxed, rehydrated, incubated in antigen

retrieval solution, and washed with Tris-buffered saline (TBS). Endogenous superoxidase was then eliminated using 0.3% H_2O_2. TBS containing 2% BSA was used to block the non-specific antibody binding (37˚C, 60 min). Then, sections were incubated overnight at 4˚C with primary antibodies against sclerostin (product code ab63097; 1:50) and Sirt1 (product code ab12193; 1:100; both from Abcam), followed by incubation (37˚C, 60 min) with biotinylated secondary antibodies (1:2,500; cat. no. ZB-2306; Beijing Zhongshan Jinqiao Biotechnology Co., Ltd.). Proteins were visualized under a light microscope using brown pigments via a standard diaminobenzidine protocol. Subsequently, slides were lightly counterstained with hematoxylin.

Serum biochemistry. Serum levels of N-terminal propeptide of type 1 procollagen (P1NP) and C-terminal crosslinked telopeptides of type I collagen (CTX-I) were measured using ELISA kits (CSB-E12775m and CSB-E12782m, respectively; Cusabio Technology LLC), following the manufacturer's instructions. Serum levels of total superoxide dismutase (t-SOD) and malondialdehyde (MDA) were quantified using commercial reagent kits (cat. nos. A001-1-2 and A003-1-2, respectively; Nanjing Jiancheng Bioengineering Institute).

Cell treatment and viability assay. MLO-Y4 cells were cultured in growth medium containing α-MEM, 2.5% CS, 2.5% FBS, 100 U/ml penicillin, and 100 μg/ml streptomycin. The cells were incubated at 37˚C in an atmosphere of 5% CO_2. The medium was changed every 2 days, and the cells were passaged after reaching 80% confluence.

During the experiment, MLO-Y4 cells were treated with various concentrations of AOPPs-BSA (from 0 to 200 μg/ml) for different durations (from 0 to 24 h), as well as co-incubated with apocynin, NAC, or SRT3025, dissolved in dimethyl sulfoxide (DMSO).

Subsequently, cell viability at different concentrations of AOPPs-BSA (50,100, 200 and 400 μg/ml) was qualitatively assessed using the fluorescein diacetate (FDA) staining assay. After washing MLO-Y4 cells three times in PBS, 5 μg/ml FDA (dissolved in DMSO) was added, and the cells were incubated at 37˚C for 10 min. Images of the live cells were captured using a model IX71 fluorescence microscope (Olympus Corporation). To quantitatively determine the effect of AOPPs-BSA on cell viability, a CCK-8 assay was performed following the manufacturer's protocol. MLO-Y4 cells were washed three times using PBS, and 10 μl CCK-8 solution was added to each well. Cells were incubated at 37˚C for 1 h and the absorbance was measured at 450 nm under a microplate reader (BioTek Instruments, Inc.).

Measurement of intracellular ROS. According to the manufacturer's instructions, intracellular ROS levels were measured in MLO-Y4 cells using a ROS assay kit (cat. no. S0033M; Beyotime Biotechnology) containing 2,7,-dichlorofluorescein diacetate (DCFH-DA) as the probe. MLO-Y4 cells under different treatment conditions (AOPPs-BSA of 0 to 200 μg/ml) were incubated with 10 μM DCFH-DA for 30 min at 37˚C. The fluorescence intensity was measured using a SpectraMax M5 microplate reader (Molecular Devices, LLC), and the fluorescence images were captured following ROS staining.

Table I. Primer sequences for real-time PCR.

Gene name	Primers
SOST	F: AGCCTTCAGGAATGATGCCAC
	R: CTTTGGCGTCATAGGGATGGT
SIRT1	F: GCTGACGACTTCGACGACG
	R: TCGGTCAACAGGAGGTTGTCT
GAPDH	F: AGGTCGGTGTGAACGGATTTG
	R: TGTAGACCATGTAGTTGAGGTCA

SOST, sclerostin; *SIRT1*, sirtuin 1; F, forward; R, reverse.

Reverse transcription-quantitative (RT-q)PCR. Total RNA of MLO-Y4 cells or femoral bone homogenate was extracted using an RNA extraction kit (Takara Bio, Inc.) and quantified using a NanoDrop 1000 spectrophotometer (Thermo Fisher Scientific, Inc.). cDNA was obtained from total RNA (50 ng), using a PrimeScript™ RT reagent kit (Takara Bio, Inc.). To quantify mRNA expression, the obtained cDNA was amplified using TB Green® Premix Ex Taq™ (TliRNaseH Plus; Takara Bio, Inc.), and qPCR was performed using a LightCycler480 system (Roche Diagnostics), following the manufacturer's instructions. Thermocycling conditions were set as follows: Incubation at 95˚C for 30 sec, amplification at 95˚C for 5 sec, 60˚C for 30 sec for a total of 40 cycles, 95˚C for 5 sec, with a final extension at 60˚C for 60 sec. The expressions levels of *Sclerostin (SOST)* and *SIRT1* genes were measured, with *GAPDH* as the reference gene. The $2^{-\Delta\Delta Cq}$ method was used for the measurement of gene expression (26). The primer sequences are listed in Table I.

Western blotting. To obtain the total cell protein, cells were rinsed with PBS at 4˚C and lysed using a cell lysis buffer (Hangzhou Fude Biological Technology Co., Ltd.). To collect the protein, the cell lysate was centrifuged at a speed of 1,2000 x g for 30 min at 4˚C. The protein concentration was determined using a BCA protein assay kit (Thermo Fisher Scientific, Inc.). Subsequently, the proteins (20 μg/lane) were separated via 6-10% SDS-PAGE, and transferred to PVDF membranes (EMD Millipore). Furthermore, the membranes were blocked (60 min at 37˚C) using 5% BSA in TBS containing 0.1% Tween-20, and incubated overnight at 4˚C with primary antibodies. The primary antibodies were directed against GAPDH (1:5,000 dilution), sclerostin (1:1,000 dilution) and Sirt1 (1:2,000 dilution). The proteins bound to the membrane were detected ECL reagent (Bio-Rad Laboratories, Inc.) after incubation with goat anti-rabbit IgG-HRP conjugated secondary antibody (product code ab205718; 1:2,000 dilution; Abcam) at 37˚C for 1 h. The integrated density of all protein bands was analyzed using ImageJ software (1.52v; National Institutes of Health).

Immunofluorescence staining. MLO-Y4 cells were washed three times using PBS and fixed for 15 min at room temperature using 4% paraformaldehyde. Following another three washes with PBS, the cells were permeabilized for 20 min at room temperature, using 1% Triton X-100/PBS

solution. Then, the cells were blocked with 5% BSA in PBS for 30 min at 37˚C. The cells were incubated overnight at 4˚C with primary rabbit anti-mouse sclerostin antibody or Sirt1 antibody (both 1:50 dilution). Primary antibodies were not added in the negative control. The following day, the primary immunoreaction was detected by incubation at 4˚C for 12 h with a Cy3-conjugated goat anti-rabbit secondary antibody (1:200 dilution). Finally, the cells were counterstained using Fluoroshield mounting medium with DAPI (37˚C, 5 min). Images were captured using IX71 fluorescence microscope (Olympus Corporation).

Statistical analysis. Data are presented as the mean ± SEM. All statistical analyses were performed using the SPSS version 22.0 (IBM Corp.). For each independent *in vitro* experiment, ≥3 technical replicates were analyzed. Differences between groups *in vivo* and *in vitro* were evaluated using one-way ANOVA, followed by post hoc least significant difference (LSD) test. For all statistical tests, $P<0.05$ was considered to indicate a statistically significant difference.

Results

AOPPs accelerate bone loss by suppressing bone formation but promoting bone resorption. The present study first measured the effect of AOPPs on bone mass and microstructure in aging mice. Compared with PBS or BSA, 50 mg/ml AOPPs-BSA significantly decreased the bone mineral density (BMD) of L4 vertebral body, and this effect was more notable in 100 mg/ml AOPPs-treated mice. However, no marked difference was observed in femoral BMD of different groups. (Fig. 1A and B). Micro-CT analysis revealed that treatment with AOPPs-BSA significantly aggravated the trabecular microstructure in aging mice. Compared with PBS or BSA-treated mice, AOPPs-treated mice displayed a significant decrease in BV/TV, Tb.N, and Tb.Th but an increase in Tb.Sp in both L4 vertebral bodies and proximal tibias. Furthermore, the degeneration of bone microstructure in the high-dose AOPPs-BSA group was greater than that in the low-dose group. (Fig. 1C-L).

To understand the effect of AOPPs on bone turnover in aging mice, the serum level of a bone formation marker (P1NP), and a bone resorption marker (CTX-1) were measured in mice of different groups. Consistent with our previous study (24), the plasma P1NP concentration was significantly decreased in mice treated with AOPPs-BSA, while the CTX-1 concentration was increased (Fig. 1M and N). Along with this finding, there was a significant decrease in the number of osteoblasts and an increase in the osteoclast area observed in the cortical diaphysis of mice treated with AOPPs-BSA, as evident by the H&E and TRAP staining, respectively (Fig. 1O-R). These data indicated that AOPPs accelerated bone deterioration in aging mice by suppressing bone formation and promoting bone resorption.

AOPPs increase sclerostin expression, and enhance OS and Sirt1 expression in mice. Sclerostin, a WNT/β-catenin inhibitor, is predominantly secreted by osteocytes (5). This protein decreases the bone mass by promoting bone resorption and suppressing bone formation (5). In the present study, it was revealed that AOPP-treated mice displayed decreased bone forming activity but increased bone resorbing activity, which was consistent with our previous study (24). These results indicated a probable involvement of sclerostin in AOPP-induced bone loss. Given that plasma sclerostin increases with age (27), the effect of AOPPs on sclerostin expression was therefore examined in aging mice. As presented in Fig. 2A, the *SOST* mRNA expression in the AOPP-treated groups was higher compared with that in PBS- or BSA-treated groups. An increased expression of sclerostin protein in mice challenged with AOPPs was also observed with immunohistochemical staining (Fig. 2B and C).

OS is regarded as a key promoting factor of osteoporosis (28). Previous studies have reported that AOPPs increase the OS status in a number of animal models (16,21,22,29). The present study evaluated the impact of AOPPs on the OS status of aging mice by testing the plasma AOPPs, MDA and t-SOD levels in femoral bone. Compared with mice treated with PBS or BSA, mice treated with AOPPs-BSA exhibited higher AOPPs and MDA levels but lower t-SOD levels (Fig. 2D-F). These results indicated that AOPPs enhanced OS in aging mice.

Sirt1 regulates sclerostin expression in osteocytes (30), and under OS status, the abundance and deacetylating activity of Sirt1 is compromised (31). Therefore, it was investigated whether there was a fluctuation of Sirt1 expression under challenge of AOPPs. As was revealed by RT-qPCR and immunohistochemical staining, Sirt1 mRNA and protein expression levels were significantly decreased in AOPP-treated mice compared with those in PBS- or BSA-treated mice (Fig. 2G-I).

Treatment with AOPPs increases sclerostin expression in MLO-Y4 cells. To investigate the effect of AOPPs on the expression of sclerostin *in vitro*, an osteocytic cell line, MLO-Y4, was used. First, the cytotoxic effect of AOPPs-BSA on MLO-Y4 cells was tested. As previously described (22,32), the viability of MLO-Y4 cells treated with different doses of AOPPs, ranging between 50-400 μg/ml, was examined. FDA staining revealed that there was only a slight decrease in the viability of cells treated with 50-200 μg/ml of AOPPs-BSA. However, cells treated with 400 μg/ml AOPPs displayed a sharp decrease in fluorescence intensity, indicating a high cytotoxic effect of AOPPs-BSA at this concentration (Fig. 3A). Furthermore, a CCK-8 assay was performed to quantify the influence of AOPPs-BSA on the viability of MLO-Y4 cells. Consistent with the FDA staining, AOPPs-BSA up to 200 μg/ml did not markedly affect cellular activity, while the absorbance value was noticeably lower in the 400 μg/ml AOPP-treated group, suggesting compromised cell viability in this group (Fig. 3B).

To evaluate the effect of AOPPs on the expression of sclerostin in MLO-Y4 cells, the cells were incubated for 24 h with AOPPs-BSA (ranging between 50-200 μg/ml). According to RT-qPCR analysis, the *SOST* mRNA expression was nearly 0.5-fold higher in the 50 μg/ml AOPPs-BSA group compared with that in the PBS group. As the concentration of AOPPs-BSA increased, the *SOST* mRNA expression levels were also increased (Fig. 3C). However, compared to the PBS group, *SOST* mRNA levels did not notably change in the BSA-treated group. The results from the western blot analysis and immunofluorescence staining further indicated that

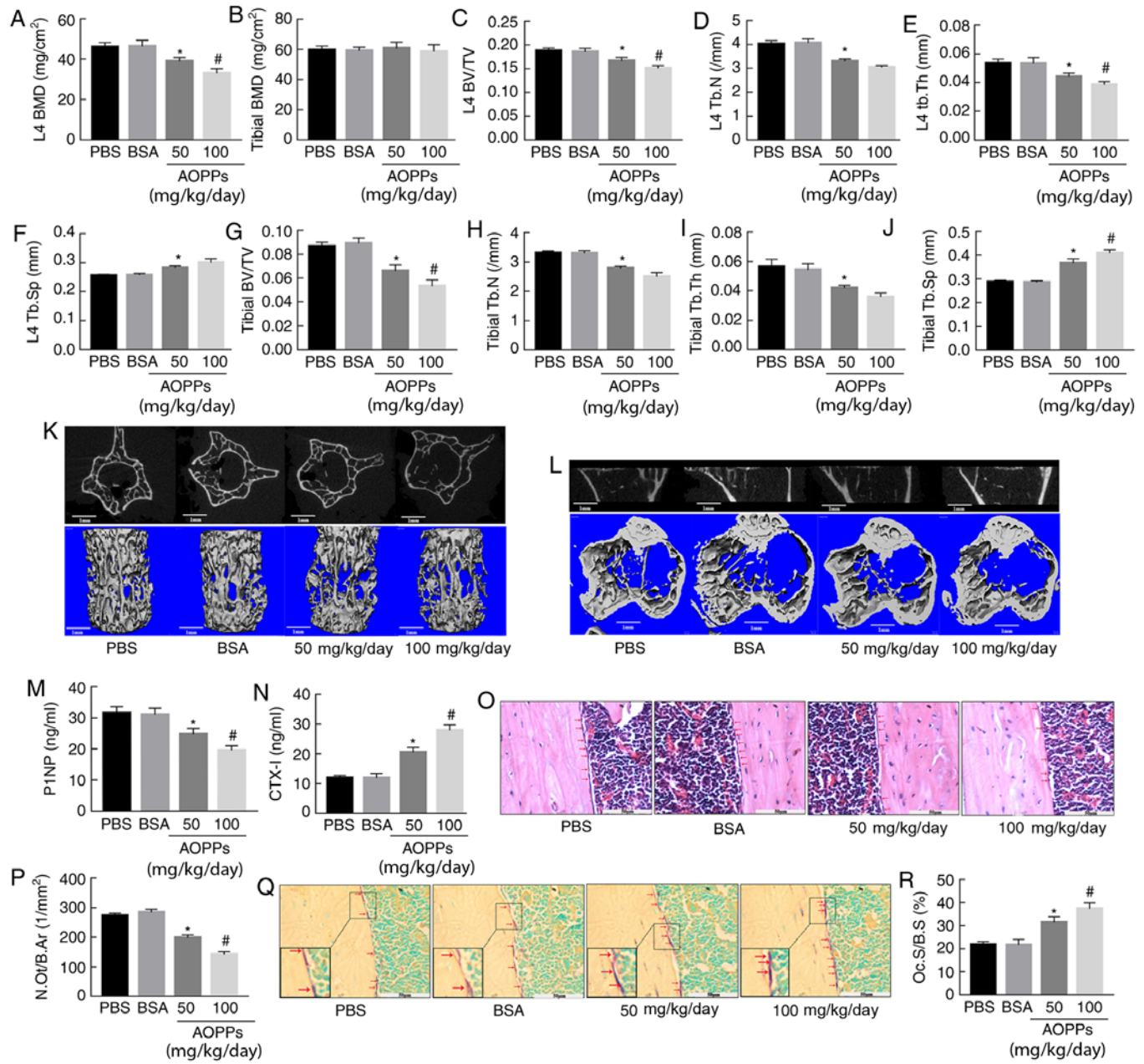

Figure 1. AOPPs accelerate bone loss by suppressing bone formation but promoting bone resorption. (A and B) AOPPs-BSA significantly decreased the BMD of the L4 vertebral body, but did not significantly affect the femoral BMD. AOPPs-BSA decreased the BV/TV, Tb.N, Tb.Th, but increased the Tb.Sp of both (C-F) L4 vertebral bodies and (G-J) proximal tibias. Representative middle cross or coronal sectional images and 3D reconstructed images of (K) L4 vertebral bodies and (L) proximal tibias in different groups. (M and N) ELISA results demonstrated that treatment with AOPPs decreased the serum P1NP levels but increased the CTX-I levels. (O and P) H&E and (Q and R) TRAP staining identified that AOPPs decreased the number of osteoblasts (red arrow) but increased the osteoclasts (red arrow) area (claret-red area) in cortical diaphysis, respectively. Magnification, x400. The data are presented as the mean ± SEM. *P<0.05 vs. the PBS or BSA group; #P<0.05 vs. the 50-mg/kg/day AOPPs-BSA group; n=7. AOPPs, advanced oxidation protein products; bovine serum albumin; BMD, bone mineral density; BV/TV, bone volume/total volume; Tb.N, trabecular number; Tb.Th, trabecular thickness; Tb.Sp, trabecular separation; P1NP, N-terminal propeptide of type 1 procollagen; CTX-I, C-terminal crosslinked telopeptides of type I collagen.

treatment with AOPPs upregulated the expression of sclerostin in MLO-Y4 cells in a dose-dependent manner (Fig. 3D and E).

AOPPs increase sclerostin expression in MLO-Y4 cells by ROS-triggered downregulation of Sirt1. Previous, including the research group of the present authors, have reported that AOPPs significantly increase the cellular ROS levels in numerous pathological processes by activating NADPH oxidases (21,22,33). Therefore, the present study examined the ROS levels in MLO-Y4 cells treated with AOPPs. Compared with PBS, BSA did not markedly affect DCFH fluorescence, which represented the intracellular ROS levels. However, 50 μg/ml AOPPs-BSA notably increased the cellular fluorescence intensity. In addition, the AOPPs-BSA-induced ROS effect was more evident in the 100- and 200-μg/ml groups (Fig. 4A and B). To investigate whether NADPH oxidases were involved in AOPP-induced ROS accumulation, MLO-Y4 cells were co-incubated with apocynin, an NADPH oxidase inhibitor. As presented in Fig. 4C, apocynin successfully decreased the ROS increase triggered by AOPPs.

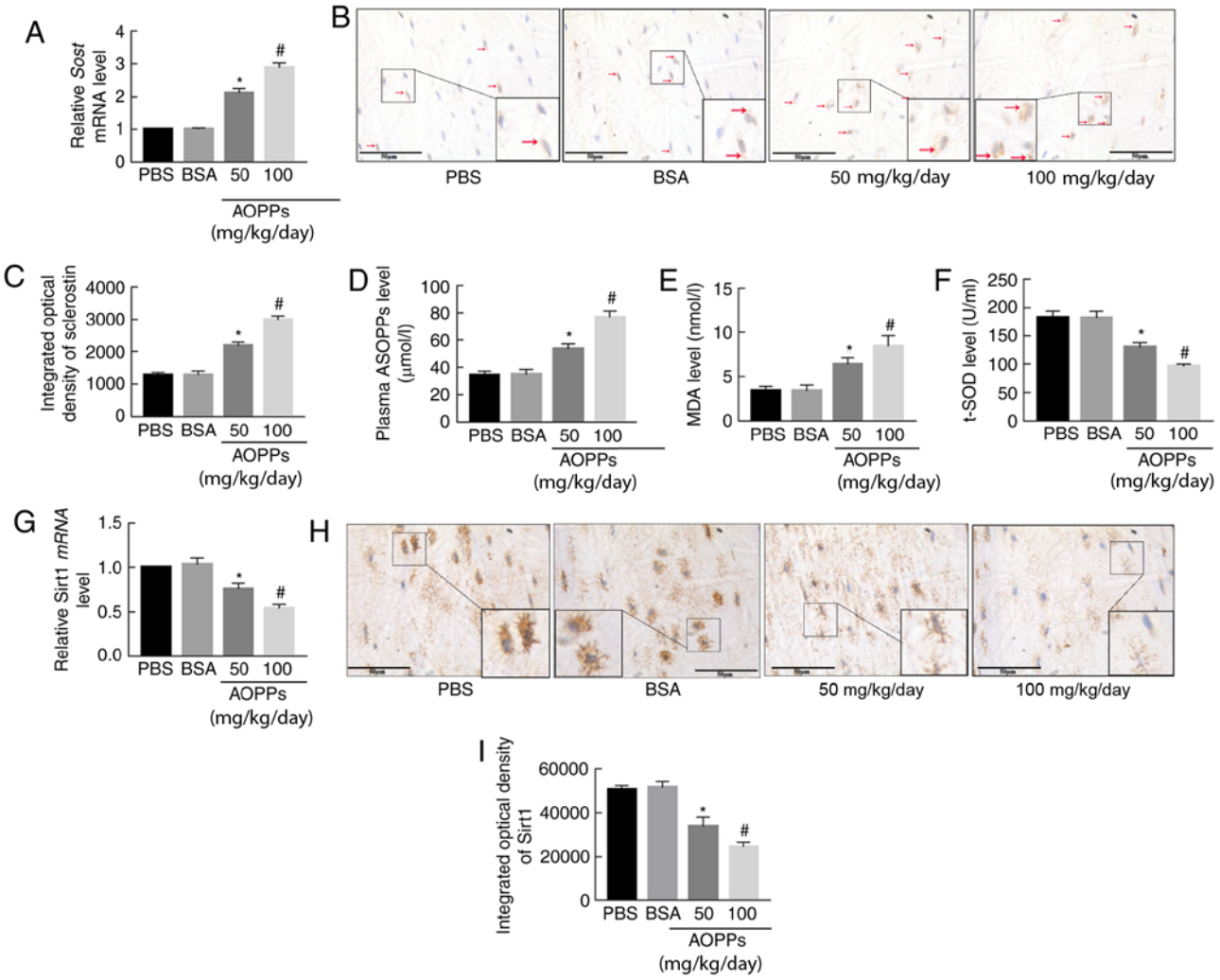

Figure 2. AOPPs increase sclerostin expression, enhance oxidative stress and downregulate Sirt1 expression in aging mice. (A) Reverse transcription-quantitative PCR results indicated that AOPPs-BSA significantly increased the mRNA expression level of *SOST* in femoral bone tissue. (B and C) Immunohistochemical staining demonstrated that sclerostin protein expression (red arrow) was significantly higher in AOPP-treated mice compared with in PBS- or BSA-treated mice. AOPPs-BSA treatment increased (D) serum levels of AOPPs and (E) MDA levels in femoral bone tissue, but (F) decreased femoral t-SOD levels. AOPPs decreased (G) *SIRT1* mRNA and (H and I) protein expression levels in femoral bone. Magnification, x400. The data are presented as the mean ± SEM. *P<0.05 vs. the PBS or BSA group; $^{\#}$P<0.05 vs. the 50-mg/kg/day AOPPs-BSA group; n=7. AOPPs, advanced oxidation protein products; Sirt1, sirtuin 1; BSA, bovine serum albumin; *SOST*, sclerostin; PBS, phosphate-buffered saline; MDA, malondialdehyde; t-SOD, total superoxide dismutase.

Evidence from previous studies has suggested that Sirt1 directly decreases the expression of sclerostin in osteocytes via epigenetic regulation (30,34,35). In addition, OS decreases Sirt1 expression in multiple diseases (31). Thus, it was investigated whether AOPPs downregulated Sirt1 expression in MLO-Y4 cells. As revealed in Fig. 4D, AOPPs significantly decreased the mRNA expression levels of *Sirt1* in a dose-dependent manner. This effect of AOPPs was further confirmed at the protein expression level, as detected via western blotting (Fig. 4E) and immunofluorescence staining (Fig. 4F). However, when the cells were co-incubated with apocynin, or a ROS scavenger, such as NAC, the aforementioned effect of AOPPs was largely blocked (Fig. 4G). These results indicated that AOPPs downregulated the expression level of Sirt1 in MLO-Y4 cells by triggering NADPH oxidase-dependent ROS accumulation.

To verify the roles of NADPH oxidases, ROS, and Sirt1 in the AOPP-induced expression of sclerostin, MLO-Y4 cells treated with AOPPs were co-incubated with apocynin, NAC, and a Sirt1 activator, SRT3025. The western blotting results demonstrated that the AOPP-induced expression of sclerostin was largely abrogated by apocynin (Fig. 4H) and NAC (Fig. 4I), whereas the expression of this protein was significantly, but not completely, diminished by SRT3025 (Fig. 4J). These results indicated that the NADPH oxidase-dependent and ROS-triggered downregulation of Sirt1 was involved in the AOPP-induced upregulation of sclerostin.

Apocynin, NAC, and SRT-3025 alleviate bone deterioration and decrease sclerostin expression in AOPP-treated mice. To further confirm the mechanism of AOPP-induced bone deterioration *in vivo*, AOPP-treated mice were co-treated with apocynin, NAC, or SRT3025. The results of the BMD measurement results identified that apocynin, NAC, and SRT3025 effectively ameliorated the loss of bone mass in L4 vertebral bodies in mice treated with AOPPs-BSA (Fig. 5A). However, the BMD of the femoral specimens was not markedly different among the various groups (Fig. 5B). Apocynin, NAC, and SRT3025 also largely alleviated the bone microstructural

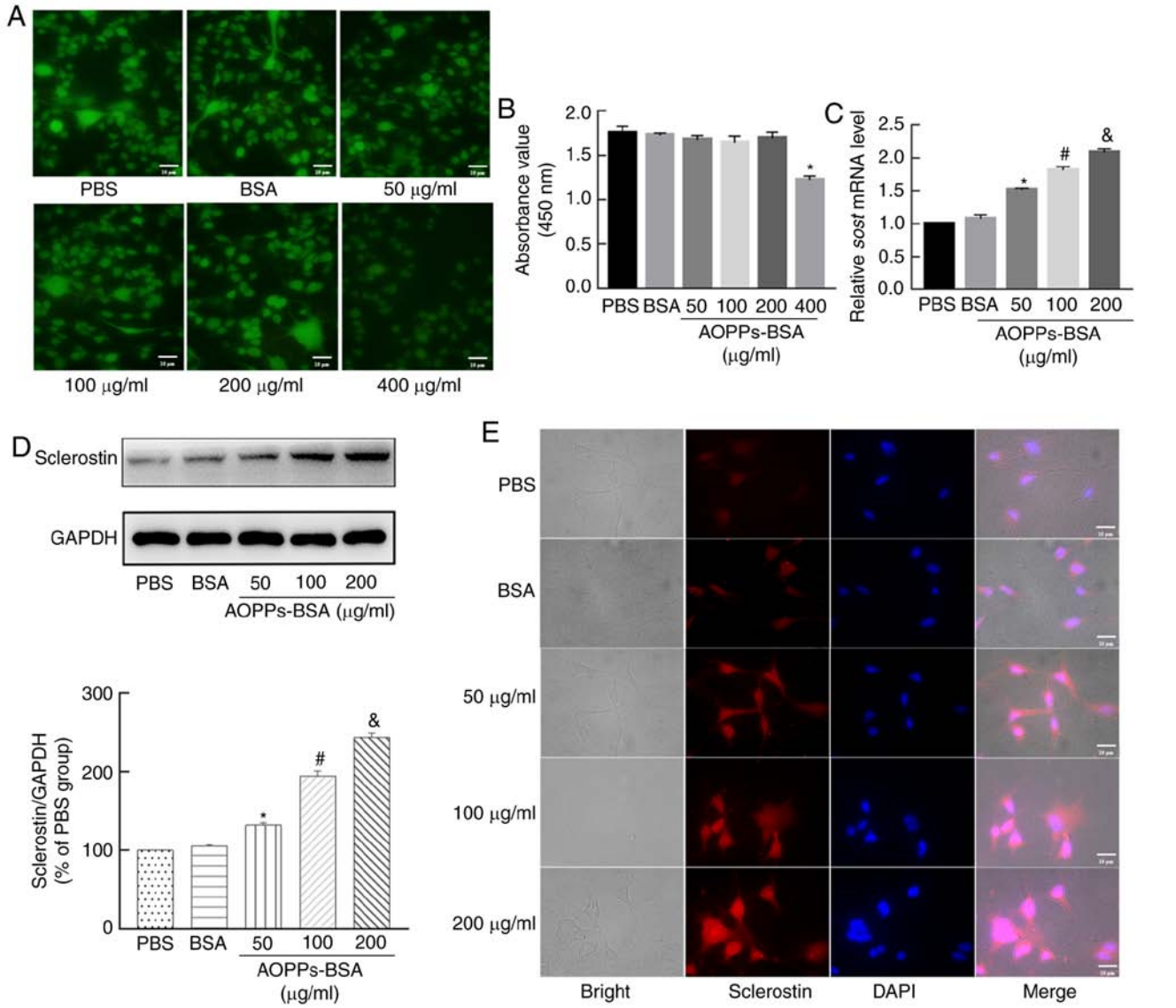

Figure 3. AOPPs increase sclerostin expression in MLO-Y4 cells. (A) Compared with the PBS or BSA group, FDA staining indicated there was only a slight decrease in cell viability in the 50, 100 and 200 μg/ml AOPPs-BSA groups. However, cell viability was significantly decreased in the 400-μg/ml AOPP-treated group. (B) The Cell Counting Kit-8 assay presented similar results. (C) Reverse transcription-quantitative PCR results demonstrated that AOPPs increased *SOST* mRNA expression in MLO-Y4 cells in a concentration-dependent manner. (D) Western blotting and (E) immunofluorescence staining revealed that AOPPs increased sclerostin protein in MLO-Y4 cells. Magnification, x400. The data are presented as the mean ± SEM. *P<0.05 vs. the PBS group; $^{\#}$P<0.05 vs. the 50-μg/ml group; $^{\&}$P<0.05 vs. the 100-μg/ml group, n=3. AOPPs, advanced oxidation protein products; PBS, phosphate-buffered saline; BSA, bovine serum albumin; FDA, fluorescein diacetate; *SOST*, sclerostin.

degeneration induced by AOPPs. As indicated by the micro-CT analyses results, the BV/TV, Tb.N and Tb.Th of L4 vertebral bodies were notably higher in the AOPPs-BSA + apocynin, AOPPs-BSA + NAC or AOPPs-BSA + SRT3025 groups compared with in the AOPPs-BSA group. However, Tb.Sp in these three groups was reduced (Fig. 5C-G). Moreover, the same microstructural changes were observed in the proximal tibias (Fig. 5H-L).

The effects of apocynin, NAC, and SRT3025 on the expression of sclerostin in the cortical bone of AOPP-treated mice were also evaluated. The RT-qPCR results demonstrated that the mRNA expression levels of *SOST* were significantly lower in the AOPPs-BSA + apocynin, AOPPs-BSA + NAC, and AOPPs + SRT3025 groups compared with in the AOPPs-BSA group (Fig. 5M). This result was also confirmed at the protein level via immunohistochemical staining (Fig. 5N and O).

Discussion

AOPPs are important proinflammatory mediators involved in the pathological processes of diverse diseases (14,22,36,37). Both animal and clinical observational studies have revealed that the plasma levels of AOPPs increase with age (23,38). However, whether AOPPs participate in the process of age-related bone loss remains unknown. Our previous study confirmed that AOPPs accelerated bone deterioration in aged rats (24). Moreover, the present study demonstrated that AOPPs aggravated the loss of bone mass and the degeneration of bone microstructure by increasing the expression level of sclerostin in osteocytes, which was mediated by ROS-dependent down-regulation of the Sirt1 pathway.

Osteocytes are the most abundant cells in bones, accounting for 90-95% of all bone cells in the adult

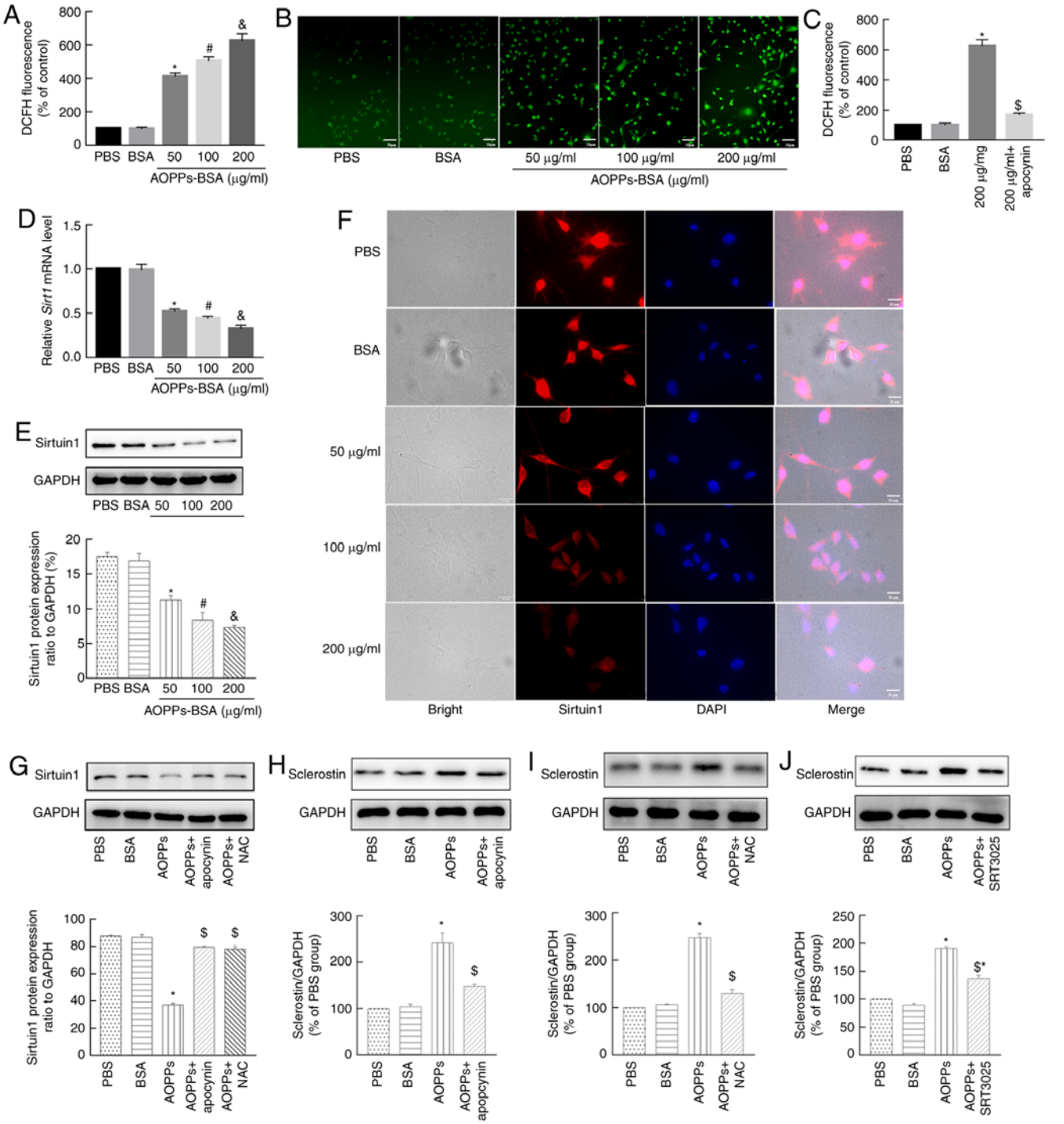

Figure 4. AOPPs increase sclerostin expression in MLO-Y4 cells via ROS-triggered downregulation of Sirt1. (A and B) AOPPs-BSA increased the intracellular ROS levels of MLO-Y4 cells, with a concentration-dependent effect. (C) Apocynin successfully eliminated the AOPP-triggered ROS accumulation. (D) *SIRT1* mRNA expression was downregulated by treatment with AOPPs, in a concentration-dependent manner. (E) This effect of AOPPs was further confirmed at the protein level via (E) western blotting and (F) immunofluorescence staining. (G) The AOPPs-induced downregulation of Sirt1 was largely blocked by apocynin or NAC. Western blotting results revealed that the AOPP-increased sclerostin expression in MLO-Y4 cells was significantly suppressed by (H) apocynin, (I) NAC, or (J) SRT3025. Magnification, x400. The data are presented as the mean ± SEM. *P<0.05 vs. the PBS group; $^{\#}$P<0.05 vs. the 50-μg/ml group; $^{\&}$P<0.05 vs. the 100-μg/ml group, $^{\$}$P<0.05 vs. the 200-$\mu$g/ml group; n=3. AOPPs, advanced oxidation protein products; ROS, reactive oxygen species; Sirt1, sirtuin 1; BSA, bovine serum albumin; NAC, N-acetyl-L-cysteine; PBS, phosphate-buffered saline.

skeleton (39). In the past decade, accumulating data have been published regarding the biology and function of osteocytes. Far from being 'passive embedded' cells, osteocytes express a series of molecules that are involved in multiple activities, especially in bone metabolism (40). Sclerostin is a cysteine-rich protein that is predominantly expressed in osteocytes and is largely considered as a negative regulator of bone formation (5,41). Sclerostin inhibits the Wnt/β-catenin signaling pathway by binding to a low-density lipoprotein receptor-related protein 5/6 (42). While genetic inactivation or mutation of the *SOST* gene, in humans and animals, results in increased bone mass, its overexpression in animals leads

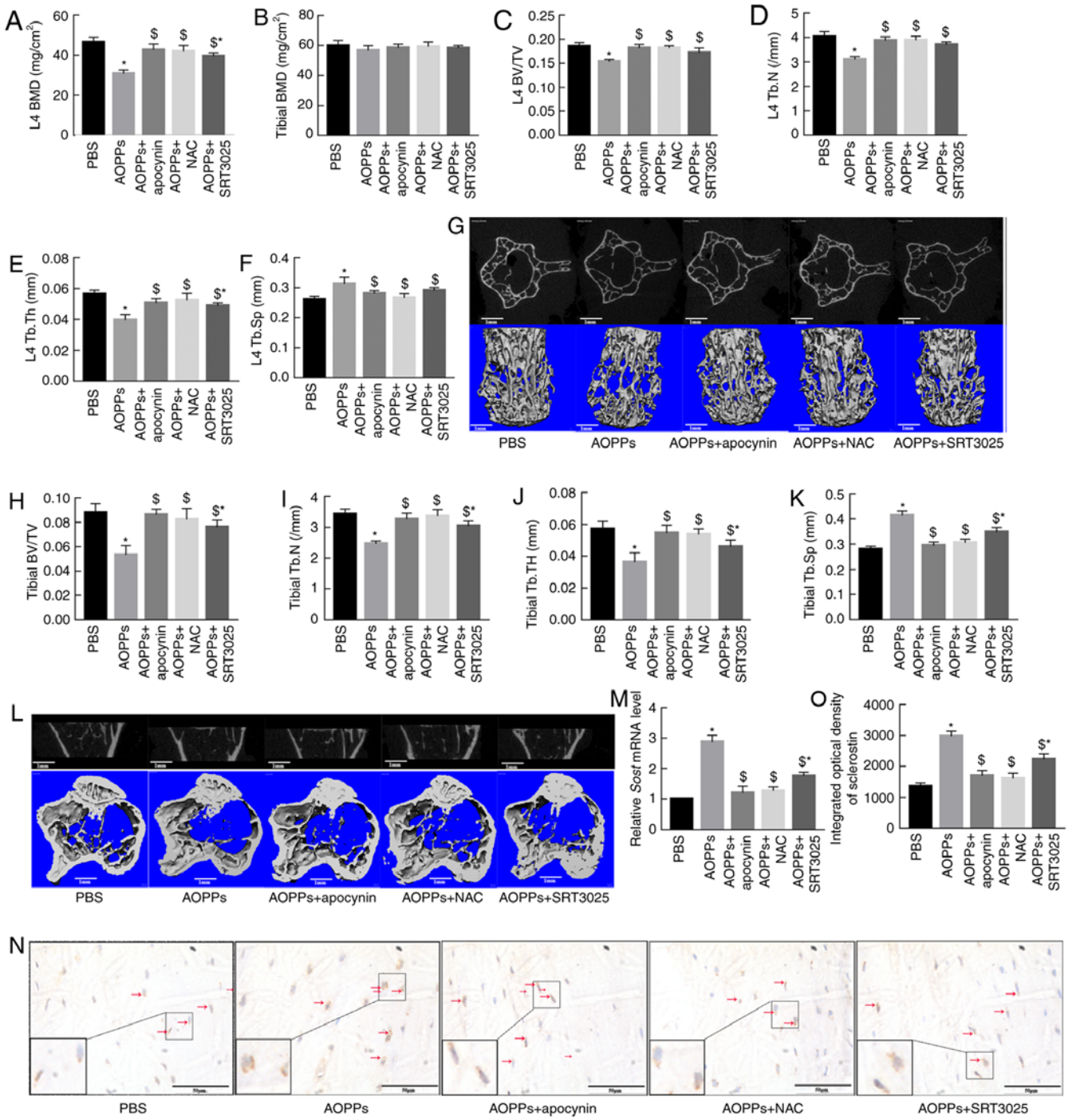

Figure 5. Apocynin, NAC and SRT3025 alleviate bone deterioration and decrease sclerostin expression in AOPP-treated mice. (A) Apocynin, NAC or SRT3025 effectively ameliorated the bone mass loss of L4 vertebral bodies in AOPP-treated mice. (B) The femoral BMD revealed no difference among different groups. Apocynin, NAC or SRT3025 improved AOPP-induced trabecular microstructural degeneration by increasing BV/TV, Tb.N and Tb.Th but by decreasing Tb.Sp in both (C-F) L4 vertebral bodies and (H-K) proximal tibias. Representative middle cross or coronal sectional images and 3D reconstructed images of (G) L4 vertebral bodies and (L) proximal tibias in different groups. (M) Reverse transcription-quantitative PCR results demonstrated that the AOPP-increased *SOST* mRNA expression was suppressed by apocynin, NAC or SRT3025. (N and O) A similar effect was confirmed at the protein level via immunohistochemical staining. Magnification, x400. The data are presented as the mean ± SEM. *P<0.05 vs. the PBS group; $^{\$}$P<0.05 vs. the 200-mg/kg/day AOPPs-BSA group; n=7. AOPPs, advanced oxidation protein products; NAC, N-acetyl-L-cysteine; BMD, bone mineral density; BV/TV, bone volume/total volume; Tb.N, trabecular number; Tb.Th, trabecular thickness; Tb.Sp, trabecular separation; *SOST*, sclerostin; PBS, phosphate-buffered saline.

to osteopenia (43-45). In a 16-month-old, gonad-intact, aged male rat model of age-related osteoporosis, 5 weeks of treatment with an antibody against sclerostin effectively restored the bone mass and strength (9). The sclerostin monoclonal antibody, romosozumab, is now an optional treatment for osteoporosis (46). Previous studies have also reported that the plasma sclerostin levels increase with age and are associated with low bone mass and osteoporotic fracture (7,8). However, the mechanism of elevated levels of sclerostin during aging are yet to be fully elucidated. In the present study, it was identified that AOPPs upregulated the expression level of sclerostin in osteocytes, both *in vitro* and *in vivo*. This result was consistent

with that of a previous study (47). Given the increased level of AOPPs with age, AOPP-induced sclerostin expression may be an important contributor to age-related bone loss.

OS is crucial in the progression of numerous diseases, including osteoporosis (48). Patients with osteoporosis are characterized by enhanced OS (28). Thus, factors that induce OS can promote osteoporosis, and when osteoporosis is improved by anti-osteoporotic treatment, the OS level also decreases (28). Previous researchers have reported that AOPPs induce OS in multiple cell types, including neutrophils, monocytes, vascular endothelial cells, mesangial cells, osteoblasts, and hepatocytes, amongst others (21,22). Consistent with these findings, the present study demonstrated that treatment with AOPPs increased MDA levels but decreased the t-SOD levels in bone tissues of AOPP-treated mice, and there was also an increase in the ROS levels in AOPP-treated cells.

NADPH oxidases are one of the main contributors of ROS. Previous studies have revealed that AOPPs induce OS mainly by activating NADPH oxidases (16). In accordance with this finding, the present study observed that the NADPH oxidase inhibitor, apocynin, effectively eliminated cellular ROS increased by AOPPs in MLO-Y4 cells.

It is important to elucidate how AOPPs influence sclerostin expression in osteocytes. Sirt1 is the most widely investigated member of the Sirt family, and serves important protective roles in age-related diseases, including osteoporosis (49,50). It has been revealed that both natural and synthetic Sirt1 activator compounds restore bone loss in animal models of osteoporosis (51). Furthermore, global or targeted deletion of Sirt1 in bone cells results in a low bone mass phenotype, while overexpression of Sirt1 protects against bone loss (50). Clinical data have suggested an association between low levels of Sirt1 and osteoporotic fractures (52). Thus, the molecular basis of Sirt1 in the regulation of bone metabolism appears complicated. In recent years, several studies have reported that Sirt1 increases bone mass by downregulating the expression of sclerostin. Sirt1 directly and negatively regulates the *SOST* gene by deacetylating histone 3 at the lysine 9 residue of the promoter (30,34,35). In the present study, treatment with AOPPs decreased the protein expression level of Sirt1 in MLO-Y4 cells, which was associated with increased sclerostin expression. Furthermore, the Sirt1 activator, SRT-3025, significantly weakened the aforementioned effects of AOPPs. However, SRT-3025 did not completely abrogate the AOPP-induced increase of sclerostin expression in MLO-Y4 cells, indicating that AOPPs increase sclerostin expression using other pathways, such as the c-Jun N-terminal kinase/p38 mitogen-activated protein kinase activation (47).

How AOPPs decrease Sirt1 expression level remains unknown. Previously published data suggest a relationship between Sirt1 and OS. While it is widely accepted that Sirt1 regulates the cellular OS burden and its toxicity, Sirt1 itself is also regulated by OS (31). For instance, both the abundance and deacetylating activity of Sirt1 decrease in response to oxidants (53,54). Similar with these findings, the present study demonstrated that AOPPs significantly suppressed Sirt1 expression via the induction of OS in MLO-Y4 cells, and this effect was effectively blocked by both the NADPH oxidase inhibitor and ROS scavenger.

Since cortical and trabecular bone does not degenerate at a same speed during aging (55), the present study is limited for not detecting the microstructural changes in cortical bone. Moreover, the sclerostin/OS/Sirt1 axis appears not to be the only axis involved in AOPP-induced bone loss. AOPPs are documented to inhibit proliferation and differentiation of osteoblasts via NF-κB pathway (32), AOPPs also induce pre-osteoblast apoptosis through a ROS-dependent, mitogen-activated protein kinase-mediated intrinsic apoptosis pathway (22). The present study is also shorted for not investigating those reported pathways.

In conclusion, the present study demonstrated that AOPPs increase sclerostin expression in osteocytes via a NADPH oxidase-dependent, ROS-triggered downregulation of the Sirt1 pathway. Therefore, the present data provide novel insights into the understanding of the pathogenic basis of senile osteoporosis.

Acknowledgements

Not applicable.

Funding

This work was supported by the National Natural Science Foundation of China (grant no. 81772395) and the Jiangxi Provincial Natural Science Foundation (grant no. 20202BAB216008).

Availability of data and materials

All data generated or analyzed during this study are included in this published article or can be obtained from the corresponding author on reasonable request.

Authors' contributions

JC and JZ conceived and designed the study. JC and QX provided administrative support. JZ and XL provided study materials. JZ and QX collected analyzed and interpreted the data. All authors wrote, read and approved the final manuscript.

Ethics approval and consent to participate

The present study was approved by the Laboratory Animal Care and Use Committee of Nanfang Hospital, Southern Medical University (approval no. NFYY-2018-68).

Patient consent for publication

Not applicable.

Competing interests

The authors declare that they have no competing interests.

References

1. Modinger Y, Loffler B, Huber-Lang M and Ignatius A: Complement involvement in bone homeostasis and bone disorders. Semin Immunol 37: 53-65, 2018.

2. Khosla S: Pathogenesis of age-related bone loss in humans. J Gerontol A Biol Sci Med Sci 68: 1226-1235, 2013.
3. Bonewald LF: The amazing osteocyte. J Bone Miner Res 26: 229-238, 2011.
4. Winkler DG, Sutherland MK, Geoghegan JC, Yu C, Hayes T, Skonier JE, Shpektor D, Jonas M, Kovacevich BR, Staehling-Hampton K, *et al*: Osteocyte control of bone formation via sclerostin, a novel BMP antagonist. EMBO J 22: 6267-6276, 2003.
5. Delgado-Calle J, Sato AY and Bellido T: Role and mechanism of action of sclerostin in bone. Bone 96: 29-37, 2017.
6. Rauch F and Adachi R: Sclerostin: More than a bone formation brake. Sci Transl Med 8: 330fs7, 2016.
7. Roforth MM, Fujita K, McGregor UI, Kirmani S, McCready LK, Peterson JM, Drake MT, Monroe DG and Khosla S: Effects of age on bone mRNA levels of sclerostin and other genes relevant to bone metabolism in humans. Bone 59: 1-6, 2014.
8. Ardawi MS, Rouzi AA, Al-Sibiani SA, Al-Senani NS, Qari MH and Mousa SA: High serum sclerostin predicts the occurrence of osteoporotic fractures in postmenopausal women: The Center of Excellence for Osteoporosis Research Study. J Bone Miner Res 27: 2592-2602, 2012.
9. Li X, Warmington KS, Niu QT, Asuncion FJ, Barrero M, Grisanti M, Dwyer D, Stouch B, Thway TM, Stolina M, *et al*: Inhibition of sclerostin by monoclonal antibody increases bone formation, bone mass, and bone strength in aged male rats. J Bone Miner Res 25: 2647-2656, 2010.
10. Finkel T: Signal transduction by reactive oxygen species. J Cell Biol 194: 7-15, 2011.
11. Schieber M and Chandel NS: ROS function in redox signaling and oxidative stress. Curr Biol 24: R453-R462, 2014.
12. Witko-Sarsat V, Friedlander M, Capeillere-Blandin C, Nguyen-Khoa T, Nguyen AT, Zingraff J, Jungers P and Descamps-Latscha B: Advanced oxidation protein products as a novel marker of oxidative stress in uremia. Kidney Int 49: 1304-1313, 1996.
13. Capeillere-Blandin C, Gausson V, Descamps-Latscha B and Witko-Sarsat V: Biochemical and spectrophotometric significance of advanced oxidized protein products. Biochim Biophys Acta 1689: 91-102, 2004.
14. Witko-Sarsat V, Friedlander M, Nguyen Khoa T, Capeillere-Blandin C, Nguyen AT, Canteloup S, Dayer JM, Jungers P, Drüeke T and Descamps-Latscha B: Advanced oxidation protein products as novel mediators of inflammation and monocyte activation in chronic renal failure. J Immunol 161: 2524-2532, 1998.
15. Wu Q, Zhong ZM, Zhu SY, Liao CR, Pan Y, Zeng JH, Zheng S, Ding RT, Lin QS, Ye Q, *et al*: Advanced oxidation protein products induce chondrocyte apoptosis via receptor for advanced glycation end products-mediated, redox-dependent intrinsic apoptosis pathway. Apoptosis 21: 36-50, 2016.
16. Xie F, Sun S, Xu A, Zheng S, Xue M, Wu P, Zeng JH and Bai L: Advanced oxidation protein products induce intestine epithelial cell death through a redox-dependent, c-jun N-terminal kinase and poly (ADP-ribose) polymerase-1-mediated pathway. Cell Death Dis 5: e1006, 2014.
17. Wu Q, Zhong ZM, Pan Y, Zeng JH, Zheng S, Zhu SY and Chen JT: Advanced oxidation protein products as a novel marker of oxidative stress in postmenopausal osteoporosis. Med Sci Monit 21: 2428-2432, 2015.
18. Kalousova M, Skrha J and Zima T: Advanced glycation end-products and advanced oxidation protein products in patients with diabetes mellitus. Physiol Res 51: 597-604, 2002.
19. Liu Z, Yao X, Jiang W, Li W, Zhu S, Liao C, Zou L, Ding R and Chen J: Advanced oxidation protein products induce microglia-mediated neuroinflammation via MAPKs-NF-κB signaling pathway and pyroptosis after secondary spinal cord injury. J Neuroinflammation 17: 90, 2020.
20. Witko-Sarsat V, Gausson V, Nguyen AT, Touam M, Drueke T, Santangelo F and Descamps-Latscha B: AOPP-induced activation of human neutrophil and monocyte oxidative metabolism: A potential target for N-acetylcysteine treatment in dialysis patients. Kidney Int 64: 82-91, 2003.
21. Sun S, Xie F, Xu X, Cai Q, Zhang Q, Cui Z, Zheng Y and Zhou J: Advanced oxidation protein products induce S-phase arrest of hepatocytes via the ROS-dependent, β-catenin-CDK2-mediated pathway. Redox Biol 14: 338-353, 2018.
22. Zhu SY, Zhuang JS, Wu Q, Liu ZY, Liao CR, Luo SG, Chen JT and Zhong ZM: Advanced oxidation protein products induce pre-osteoblast apoptosis through a nicotinamide adenine dinucleotide phosphate oxidase-dependent, mitogen-activated protein kinases-mediated intrinsic apoptosis pathway. Aging Cell 17: e12764, 2018.
23. Zhang YB, Zhong ZM, Hou G, Jiang H and Chen JT: Involvement of oxidative stress in age-related bone loss. J Surg Res 169: e37-42, 2011.
24. Zeng JH, Zhong ZM, Li XD, Wu Q, Zheng S, Zhou J, Ye WB, Xie F, Wu XH, Huang ZP and Chen JT: Advanced oxidation protein products accelerate bone deterioration in aged rats. Exp Gerontol 50: 64-71, 2014.
25. Bouxsein ML, Boyd SK, Christiansen BA, Guldberg RE, Jepsen KJ and Muller R: Guidelines for assessment of bone microstructure in rodents using micro-computed tomography. J Bone Miner Res 25: 1468-1486, 2010.
26. Livak KJ and Schmittgen TD: Analysis of relative gene expression data using real-time quantitative PCR and the 2(-Delta Delta C(T)) method. Method 25: 402-408, 2001.
27. Coulson J, Bagley L, Barnouin Y, Bradburn S, Butler-Browne G, Gapeyeva H, Hogrel JY, Maden-Wilkinson T, Maier AB, Meskers C, *et al*: Circulating levels of dickkopf-1, osteoprotegerin and sclerostin are higher in old compared with young men and women and positively associated with whole-body bone mineral density in older adults. Osteoporos Int 28: 2683-2689, 2017.
28. Manolagas SC: From estrogen-centric to aging and oxidative stress: A revised perspective of the pathogenesis of osteoporosis. Endocr Rev 31: 266-300, 2010.
29. Shi XY, Hou FF, Niu HX, Wang GB, Xie D, Guo ZJ, Zhou ZM, Yang F, Tian JW and Zhang X: Advanced oxidation protein products promote inflammation in diabetic kidney through activation of renal nicotinamide adenine dinucleotide phosphate oxidase. Endocrinology 149: 1829-1839, 2008.
30. Cohen-Kfir E, Artsi H, Levin A, Abramowitz E, Bajayo A, Gurt I, Zhong L, D'Urso A, Toiber D, Mostoslavsky R and Dresner-Pollak R: Sirt1 is a regulator of bone mass and a repressor of Sost encoding for sclerostin, a bone formation inhibitor. Endocrinology 152: 4514-4524, 2011.
31. Hwang JW, Yao H, Caito S, Sundar IK and Rahman I: Redox regulation of SIRT1 in inflammation and cellular senescence. Free Radic Biol Med 61: 95-110, 2013.
32. Zhong ZM, Bai L and Chen JT: Advanced oxidation protein products inhibit proliferation and differentiation of rat osteoblast-like cells via NF-kappaB pathway. Cell Physiol Biochem 24: 105-114, 2009.
33. Ding R, Jiang H, Sun B, Wu X, Li W, Zhu S, Liao C, Zhong Z and Chen J: Advanced oxidation protein products sensitized the transient receptor potential vanilloid 1 via NADPH oxidase 1 and 4 to cause mechanical hyperalgesia. Redox Biol 10: 1-11, 2016.
34. Artsi H, Cohen-Kfir E, Gurt I, Shahar R, Bajayo A, Kalish N, Bellido TM, Gabet Y and Dresner-Pollak R: The Sirtuin1 activator SRT3025 down-regulates sclerostin and rescues ovariectomy-induced bone loss and biomechanical deterioration in female mice. Endocrinology 155: 3508-3515, 2014.
35. Stegen S, Stockmans I, Moermans K, Thienpont B, Maxwell PH, Carmeliet P and Carmeliet G: Osteocytic oxygen sensing controls bone mass through epigenetic regulation of sclerostin. Nat Commun 9: 2557, 2018.
36. Liu SX, Hou FF, Guo ZJ, Nagai R, Zhang WR, Liu ZQ, Zhou ZM, Zhou M, Xie D, Wang GB and Zhang X: Advanced oxidation protein products accelerate atherosclerosis through promoting oxidative stress and inflammation. Arterioscler Thromb Vasc Biol 26: 1156-1162, 2006.
37. Li HY, Hou FF, Zhang X, Chen PY, Liu SX, Feng JX, Liu ZQ, Shan YX, Wang GB, Zhou ZM, *et al*: Advanced oxidation protein products accelerate renal fibrosis in a remnant kidney model. J Am Soc Nephrol 18: 528-538, 2007.
38. Komosinska-Vassev K, Olczyk P, Winsz-Szczotka K, Kuznik-Trocha K, Klimek K and Olczyk K: Age- and gender-related alteration in plasma advanced oxidation protein products (AOPP) and glycosaminoglycan (GAG) concentrations in physiological ageing. Clin Chem Lab Med 50: 557-563, 2012.
39. Bonewald LF: Osteocytes as dynamic multifunctional cells. Ann N Y Acad Sci 1116: 281-290, 2007.
40. Dallas SL, Prideaux M and Bonewald LF: The osteocyte: An endocrine cell ... and more. Endocr Rev 34: 658-690, 2013.
41. van Bezooijen RL, ten Dijke P, Papapoulos SE and Lowik CW: SOST/sclerostin, an osteocyte-derived negative regulator of bone formation. Cytokine Growth Factor Rev 16: 319-327, 2005.
42. Li XF, Zhang Y, Kang H, Liu W, Liu P, Zhang J, Harris SE and Wu D: Sclerostin binds to LRP5/6 and antagonizes canonical Wnt signaling. J Biol Chem 280: 19883-19887, 2005.
43. Balemans W, Patel N, Ebeling M, Van Hul E, Wuyts W, Lacza C, Dioszegi M, Dikkers FG, Hildering P, Willems PJ, *et al*: Identification of a 52 kb deletion downstream of the SOST gene in patients with van Buchem disease. J Med Genet 39: 91-97, 2002.

44. Balemans W, Ebeling M, Patel N, Van Hul E, Olson P, Dioszegi M, Lacza C, Wuyts W, Van Den Ende J, Willems P, *et al*: Increased bone density in sclerosteosis is due to the deficiency of a novel secreted protein (SOST). Hum Mol Genet 10: 537-543, 2001.
45. Zhang D, Park BM, Kang M, Nam H, Kim EJ, Bae C and Lim SK: The systemic effects of sclerostin overexpression using ΦC31 integrase in mice. Biochem Biophys Res Commun 472: 471-476, 2016.
46. Cosman F, Crittenden DB, Adachi JD, Binkley N, Czerwinski E, Ferrari S, Hofbauer LC, Lau E, Lewiecki EM, Miyauchi A, *et al*: Romosozumab treatment in postmenopausal women with osteoporosis. N Engl J Med 375: 1532-1543, 2016.
47. Yu C, Huang D, Wang K, Lin B, Liu Y, Liu S, Wu W and Zhang H: Advanced oxidation protein products induce apoptosis, and upregulate sclerostin and RANKL expression, in osteocytic MLO-Y4 cells via JNK/p38 MAPK activation. Mol Med Rep 15: 543-550, 2017.
48. Finkel T and Holbrook NJ: Oxidants, oxidative stress and the biology of ageing. Nature 408: 239-247, 2000.
49. Baur JA, Ungvari Z, Minor RK, Le Couteur DG and de Cabo R: Are sirtuins viable targets for improving healthspan and lifespan? Nat Rev Drug Discov 11: 443-461, 2012.
50. Zainabadi K: Drugs targeting SIRT1, a new generation of therapeutics for osteoporosis and other bone related disorders? Pharmacol Res 143: 97-105, 2019.
51. Kim HN, Han L, Iyer S, de Cabo R, Zhao H, O'Brien CA, Manolagas SC and Almeida M: Sirtuin1 suppresses osteoclastogenesis by deacetylating FoxOs. Mol Endocrinol 29: 1498-1509, 2015.
52. El-Haj M, Gurt I, Cohen-Kfir E, Dixit V, Artsi H, Kandel L, Yakubovsky O, Safran O and Dresner-Pollak R: Reduced Sirtuin1 expression at the femoral neck in women who sustained an osteoporotic hip fracture. Osteoporos Int 27: 2373-2378, 2016.
53. Caito S, Rajendrasozhan S, Cook S, Chung S, Yao H, Friedman AE, Brookes PS and Rahman I: SIRT1 is a redox-sensitive deacetylase that is post-translationally modified by oxidants and carbonyl stress. Faseb J 24: 3145-3159, 2010.
54. Furukawa A, Tada-Oikawa S, Kawanishi S and Oikawa S: H_2O_2 accelerates cellular senescence by accumulation of acetylated p53 via decrease in the function of SIRT1 by NAD^+ depletion. Cell Physiol Biochem 20: 45-54, 2007.
55. Farr JN and Khosla S: Skeletal changes through the lifespan-from growth to senescence. Nat Rev Endocrinol 11: 513-521, 2015.